ACS ORGANIC & INORGANIC Au
AN OPEN ACCESS JOURNAL OF THE AMERICAN CHEMICAL SOCIETY

pubs.acs.org/orginorgau
Article

NO Generation from Nitrite at Zinc(II): Role of Thiol Persulfidation in the Presence of Sulfane Sulfur

Tuhin Sahana, Adwaith K. Valappil, Anaswar S. P. R. Amma, and Subrata Kundu*

Cite This: *ACS Org. Inorg. Au* 2023, 3, 246−253
Read Online
ACCESS | Metrics & More | Article Recommendations | Supporting Information

ABSTRACT: Nitrite-to-NO transformation is of prime importance due to its relevance in mammalian physiology. Although such a one-electron reductive transformation at various redox-active metal sites (e.g., Cu and Fe) has been illustrated previously, the reaction at the [Zn^{II}] site in the presence of a sacrificial reductant like thiol has been reported to be sluggish and poorly understood. Reactivity of [(**Bn_3Tren**)Zn^{II}−ONO](ClO_4) (**1**), a nitrite-bound model of the tripodal active site of carbonic anhydrase (CA), toward various organic probes, such as 4-*tert*-butylbenzylthiol (^{t}BuBnSH), 2,4-di-*tert*-butylphenol (2,4-DTBP), and 1-fluoro-2,4-dinitrobenzene (F-DNB), reveals that the ONO-moiety in the [Zn^{II}]−nitrite coordination motif of complex **1** acts as a mild electrophile. ^{t}BuBnSH reacts mildly with nitrite at a [Zn^{II}] site to provide *S*-nitrosothiol ^{t}BuBnSNO prior to the release of NO in 10% yield, whereas the phenolic substrate 2,4-DTBP does not yield the analogous *O*-nitrite compound (ArONO). The presence of sulfane sulfur (S^0) species such as elemental sulfur (S_8) and organic polysulfides (^{t}BuBnS_nBn^{t}Bu) during the reaction of ^{t}BuBnSH and [Zn^{II}]−nitrite (**1**) assists the nitrite-to-NO conversion to provide NO yields of 65% (for S_8) and 76% (for ^{t}BuBnS_nBn^{t}Bu). High-resolution mass spectrometry (HRMS) analyses on the reaction of [Zn^{II}]−nitrite (**1**), ^{t}BuBnSH, and S_8 depict the formation of zinc(II)-persulfide species [(**Bn_3Tren**)Zn^{II}−S_n−Bn^{t}Bu]$^+$ (where n = 2, 3, 4, 5, and 6). Trapping of the persulfide species (^{t}BuBnSS$^-$) with 1-fluoro-2,4-dinitrobenzene (F-DNB) confirms its intermediacy. The significantly higher nucleophilicity of persulfide species (relative to thiol/thiolate) is proposed to facilitate the reaction with the mildly electrophilic [Zn^{II}]−nitrite (**1**) complex. Complementary analyses, including multinuclear NMR, electrospray ionization-MS, UV−vis, and trapping of reactive S-species, provide mechanistic insights into the sulfane sulfur-assisted reactions between thiol and nitrite at the tripodal [Zn^{II}]-site. These findings suggest the critical influential roles of various reactive sulfur species, such as sulfane sulfur and persulfides, in the nitrite-to-NO conversion.

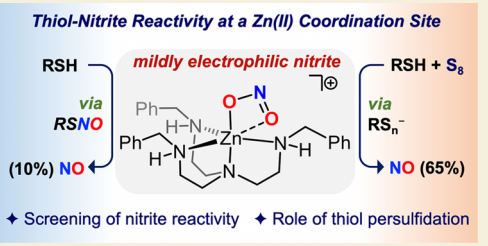

KEYWORDS: *zinc(II), nitrite, nitric oxide, thiol, sulfane sulfur, persulfidation*

INTRODUCTION

Nitrite (NO_2^-) anion plays pivotal roles in nitric oxide (NO) signaling pathways in mammalian physiology.[1,2] Interconversion between NO_2^- and NO in the biological milieu renders NO_2^- to be a sink as well as a reservoir of NO, depending on the cellular microenvironment.[1,2] For instance, the oxidized form of heme-Fe/Cu-containing cytochrome *c* oxidase (C*c*O) mediates NO monooxygenation to NO_2^- under normoxia, while the reduced form of C*c*O assists the reverse transformation under hypoxic conditions (Figure 1A).[2] Thus, NO generated from the reduction of NO_2^- supports recovery from hypoxia through amplifying blood oxygenation and vasodilation.[3] Although nitrite reductase (NiR) activity in prokaryotic organisms is mediated by heme-Fe-containing cd_1NiR and Cu-containing CuNiR (Figure 1B),[2,4] the analogous transformations in mammals are carried out by various heme-Fe-containing proteins, including deoxy-hemoglobin (Hb)/-myoglobin (Mb) and the Mo site of xanthine/aldehyde oxidase (XO/AO) (Figure 1C).[5,6]

Strikingly, NO generation from nitrite at a redox-inactive [Zn^{II}] site of carbonic anhydrase (CA) has also been reported in the literature.[7] $(His)_3Zn^{II}$-aqua active site of CA primarily maintains the pH of blood through CO_2 hydration (CO_2 + H_2O ⇄ HCO_3^- + H^+) and thus controls the O_2 affinity of blood, commonly known as the Bohr effect. Notably, the NO_2^- anion has been known to inhibit the CA activity through binding at the [Zn^{II}] site.[8] The mechanism of NO_2^- to NO conversion at the CA active site has been postulated to proceed via a redox-neutral dehydration of HNO_2 (the conjugate acid of NO_2^-) to a metastable species N_2O_3, followed by metal-free homolysis to NO and NO_2 (Figure 1D).[7] Contrastingly, several recent studies revisiting the CA-mediated NO_2^- to NO transformation suggest that CA serves neither as nitrite reductase nor as anhydrase.[9−11] NO generation from NO_2^- at the CA active site in the absence

Received: February 10, 2023
Revised: May 30, 2023
Accepted: May 31, 2023
Published: June 14, 2023

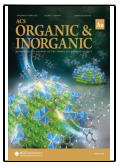

https://doi.org/10.1021/acsorginorgau.3c00004
ACS Org. Inorg. Au 2023, 3, 246−253

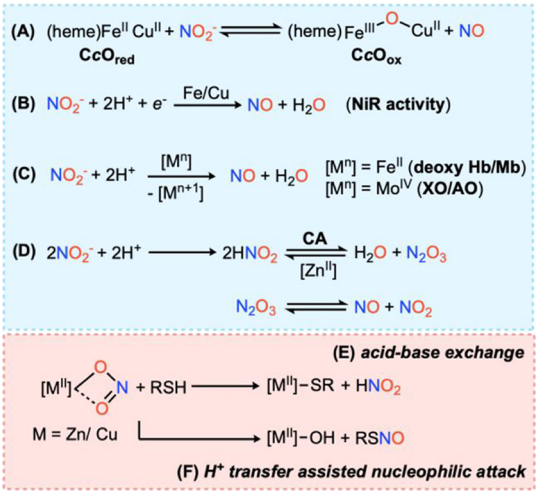

Figure 1. Nitrite to NO transformation at various metalloenzyme active sites (A–D) and representative routes for the thiol-mediated reactions of Cu^{II}/Zn^{II}–nitrite model complexes (E,F). Abbreviations: $Cc O_{red/ox}$—cytochrome *c* oxidase reduced/oxidized forms, NiR—nitrite reductase, Hb/Mb—hemoglobin/myoglobin, XO/AO—xanthine/aldehyde oxidase, CA—carbonic anhydrase.

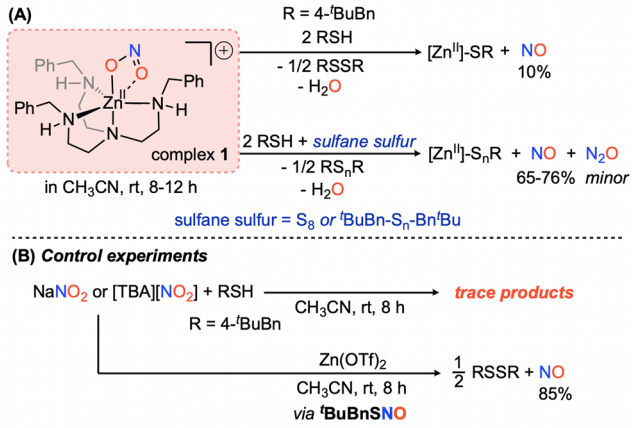

Figure 2. Reactions of thiol with nitrite. Figure 3 and Table S1 represent the distribution of nitrogen-oxide products resultant from the above-reactions.

of a sacrificial reductant remains disputed, while detailed investigations, including ^{15}N-isotope labeling studies on the CA-mediated reactions of $^{15}NO_2^-$ in the presence of glutathione (GSH), clearly suggest the formation of *S*-nitrosoglutathione ($GS^{15}NO$).[12] Employing a synthetic model of the CA active site, namely [(^{iPr2}Tp)Zn^{II}(κ^2-*O*:*O*′-nitrite)] (where, Tp = tris(pyrazolyl)borate),[13] Warren et al. have demonstrated that thiol (RSH) reacts with the [Zn^{II}]–nitrite, presumably through an acid–base exchange route to yield [Zn^{II}]–SR and HNO_2 (Figure 1E). Subsequently, HNO_2 is proposed to nitrosate RSH, affording *S*-nitrosothiol (RSNO). Alternatively, an electrophilic nitrite moiety at a [Cu^{II}] site supported by an electron-deficient β-diketiminato ligand has been illustrated to follow concerted nitrosation of RSH to RSNO through proton-transfer assisted nucleophilic attack (Figure 1F).[14] Interestingly, nitrite bound at the heme-Fe^{III} site has been demonstrated to react with cysteine (CysSH) to yield the sulfenic acid derivative CysS(O)H through oxygen atom transfer (OAT).[15] In contrast, a reaction of the nonheme-Fe^{II}(dinitrite) complex with RSH affording disulfide (RSSR) and NO has been shown to proceed through an initial protonation of the nitrite moiety.[16] Although the transformation of NO_2^- to NO at various redox-active transition metals such as Fe/Co/Ni/Cu has been relatively well explored in the presence of a diverse array of exogenous reductants (e.g., phosphine, CO, VCl_3, thiol, phenol, and enediols),[17−23] the examples of analogous reactions at a redox-inactive [Zn^{II}] site and the underlying factors for promoting the reaction remain poorly understood. Notably, the NO-releasing reactions of [Zn^{II}]–nitrite complexes in the presence of external reductants like benzylthiol and 3,5-di-*tert*-butylcatechol have been reported to be slow.[13,23] Herein, this report investigates the thiol reactivity of a previously reported CA-model bound to nitrite,[23] namely [(**Bn_3Tren**)Zn^{II}(κ^2-*O*:*O*′-nitrite)](ClO_4) (**1**) (Figure 2), aiming to disclose biologically relevant conditions for an efficient transformation of nitrite-to-NO at a zinc(II) site. The reactivity of the [Zn^{II}]–nitrite complex (**1**) with thiol toward NO generation has found to be sluggish due to the poor Lewis acidity of the [Zn^{II}] site in **1**. However, the presence of sulfane sulfur (S^0) species (e.g., elemental sulfur (S_8) and polysulfides (RS_nR, $n > 2$) during the reactions of [Zn^{II}]–nitrite (**1**) and thiol leads to a significantly higher yield of NO due to the more facile nucleophilic attack of the in-situ-generated reactive persulfide (RSS^-) species.[24]

RESULTS AND DISCUSSION

Reactions of Thiol toward Nitrite at Zinc(II)

An equimolar reaction of [Zn^{II}]–nitrite complex [(**Bn_3Tren**)-Zn^{II}(κ^2-*O*:*O*′-nitrite)](ClO_4) (**1**) with 4-*tert*-butylbenzylthiol (^{t}BuBnSH) in acetonitrile at room temperature shows only 18% consumption of thiol along with the generation of *S*-nitrosothiol (^{t}BuBnSNO) and disulfide (^{t}BuBnSSBn^{t}Bu) as assessed by ^1H NMR resonances at δ = 4.71 and 3.60 ppm, respectively (Figures 2 and S1). Notably, the nitrite anion in $NaNO_2$ or [TBA][NO_2] salts does not react with ^{t}BuBnSH under these reaction conditions (Figures S1 and S2). In the presence of $Zn(OTf)_2$ or $Zn(ClO_4)_2{\cdot}6H_2O$ salt, however, the reaction of sodium nitrite and ^{t}BuBnSH results in a distinct pink-colored solution. The UV–vis absorption spectrum of the crude reaction mixture reveals an absorption feature at λ_{max} = 550 nm, which is attributed to an $n_N \rightarrow \pi^*$ electronic transition of ^{t}BuBnSNO (Figure S3).[25] FTIR spectra of the crude reaction mixtures obtained from the reactions of $Zn(OTf)_2$ + $NaNO_2$ (or $Na^{15}NO_2$) + ^{t}BuBnSH show an N-isotope-sensitive vibrational feature at 1510 (1479) cm^{-1}, which is in the range as previously reported for *S*-nitrosothiol (Figure S4).[26] Furthermore, the ^{15}N NMR spectrum of the ^{15}N-enriched sample in CD_3CN at −30 °C depicts a sharp resonance at 758 ppm (versus liq. NH_3) (Figure S5), thereby confirming the generation of ^{t}BuBn$S^{15}NO$ from the Zn(II)-mediated reaction of ^{15}N-nitrite and ^{t}BuBnSH.[26] A ^1H NMR spectroscopic study on the reaction mixture depicts full consumption of ^{t}BuBnSH and indeed confirms the formation of ^{t}BuBnSNO and ^{t}BuBnSSBn^{t}Bu (Figure S6). The disulfide from the above-mentioned reactions forms through the thermal homolysis of the S–N bond (BDE_{S-N} = ∼30 kcal/mol) in ^{t}BuBnSNO and is accompanied by NO generation.[25,27] Analyses of the headspace on the thiol reactions with [(**Bn_3Tren**)Zn^{II}–nitrite]$^+$ complex (**1**) and {$NaNO_2$ + $Zn^{II}(OTf)_2$} provide 10 and 85% yields of NO (Table S1), respectively, as obtained from diffusion-controlled trapping

https://doi.org/10.1021/acsorginorgau.3c00004
ACS Org. Inorg. Au 2023, 3, 246−253

experiments employing (TPP)Co^{II} (TPP = tetraphenyl porphyrin) as a well-established NO-trap (Figure S7).[23] In addition, UV−vis spectrophotometric estimations of nitrite in each of the reaction mixture of ^{t}BuBnSH with complex **1** or $NaNO_2$ or {$NaNO_2$ + $Zn(OTf)_2$} using Griess assay provide the presence of 74, 95%, and a trace amount of unreacted nitrite after the reactions, respectively (Figures 2 and 3 and

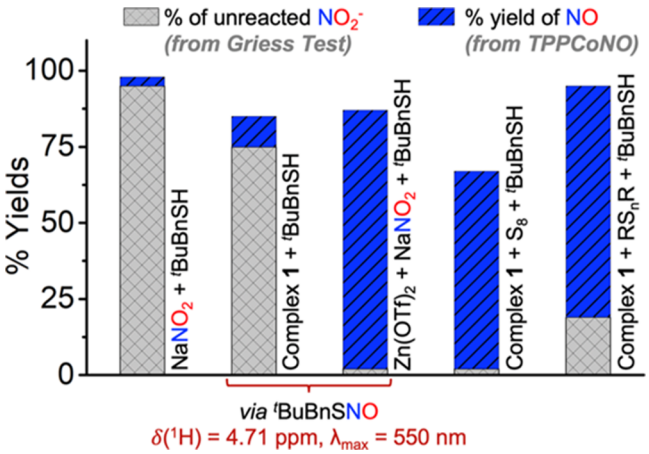

Figure 3. Comparison of the yields of NO from the reactions of thiol with nitrite.

Table S1).[28] Thus, the quantifications of unreacted NO_2^- and generated NO in the above-mentioned reactions are consistent with the consumption of alkyl thiol RSH leading to RSNO and RSSR. A reaction of a relatively more acidic aryl thiol such as 4-methylbenzenethiol (4-Me−C_6H_4−SH) with the [Zn^{II}]−nitrite complex (**1**) provides 30% unreacted nitrite and 39% NO (Figure S8). While the conversion of nitrite to NO in the presence of aryl thiol is relatively more efficient as compared to alkyl thiol (Figure S8), a ^{1}H NMR spectroscopic study does not show the presence of 4-Me−C_6H_4−SNO perhaps due to the metastable nature of ArSNO. Notably, a reaction of 4-Me−C_6H_4−SH with $NaNO_2$ in the presence of $Zn(OTf)_2$ provides a near quantitative yield of NO via dark brownish-green colored transient species 4-Me−C_6H_4−SNO featuring λ_{max} = 570 nm (Figures S3 and S8).

Reactivity Profile of Nitrite at [Zn^{II}] versus in $NaNO_2$

Illustrating the differences in the yield of NO from nitrite in complex **1** versus {$NaNO_2$ + $Zn(OTf)_2$} versus $NaNO_2$, we turned to probe the nature of the nitrite moiety employing the concept of nucleophilic and electrophilic aromatic substitution reactions. The nucleophilic and electrophilic reactivity profiles have been assessed using electron-deficient 1-fluoro-2,4-dinitrobenzene (F-DNB) and electron-rich 2,4-di-*tert*-butylphenol (2,4-DTBP) as the substrates, respectively (Figure 4). ^{1}H NMR spectrum of a crude mixture obtained from a reaction of tetrabutylammonium nitrite [TBA^+][NO_2^-] and F-DNB (2 equiv) shows the formation of 2,4-dinitrophenol in 72% yield w.r.t. nitrite (Figures S9 and S10),[29] thereby demonstrating nucleophilic aromatic substitution. ^{15}N NMR of the reaction mixture consisting of ^{15}N-enriched [TBA^+][$^{15}NO_2^-$] and F-DNB depicts the formation of the *O*-nitrite species O^{15}NO-DNB with $\delta(^{15}N)$ at 587 ppm (versus liq. NH_3) as a transient intermediate prior to yield 2,4-dinitrophenol (Figure S11).[30] Furthermore, UV−vis monitoring of the reaction of [TBA^+]-[NO_2^-] and F-DNB in acetonitrile at room temperature

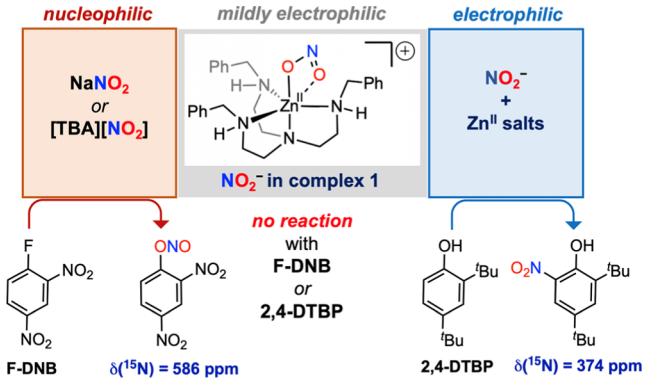

Figure 4. Screening of the reactivity of nitrite as a nucleophile versus an electrophile. See Scheme S1 for details.

displays a growth of two transient absorption features at 350 and 425 nm, which subsequently decompose (Figure S12). These UV−vis and multinuclear NMR spectroscopic studies suggest the formation of *O*-nitrite through the facile nucleophilic attack by the uncoordinated NO_2^- anion on F-DNB. In contrast, [(**Bn_3Tren**)Zn^{II}−nitrite]$^+$ (**1**) does not react with F-DNB (Figure 4), thereby illustrating the non-nucleophilic nature of the nitrite moiety in **1** (Figures S12 and S13). Moreover, NO_2^- anion in the presence of [Zn^{II}] salts such as $Zn(OTf)_2$ or $Zn(ClO_4)_2{\cdot}6H_2O$ does not react with F-DNB, presumably due to the interactions of the negative charge density of the nitrite anion with the zinc(II) site, thereby quenching the nucleophilicity.

Neither [(**Bn_3Tren**)Zn^{II}−nitrite]$^+$ (**1**) nor $NaNO_2$ react with 2,4-DTBP at room temperature to provide nitro-derivative 6-nitro-2,4-DTBP, while a solution containing a mixture of $NaNO_2$ and $Zn(OTf)_2$ reacts with 2,4-DTBP to afford 6-nitro-2,4-DTBP (38%) (Figures 4 and S14).[21] Likewise, 1,2,4-trimethoxybenzene (1,2,4-TMB) reacts with a mixture of $NaNO_2$ and $Zn(OTf)_2$ to yield 1,2,4-trimethoxy-5-nitrobenzene (21%),[31] although complex **1** does not react with 1,2,4-TMB (Figure S15). ^{15}N NMR spectroscopic studies on the sample generated from the reactions of $Zn(OTf)_2$ + $Na^{15}NO_2$ + 2,4-DTBP (or 1,2,4-TMB) depict the ^{15}N-chemical shifts $\delta(^{15}N)$ at 374 (or 368) ppm consistent with the nitrations of 2,4-DTBP and 1,2,4-TMB, respectively (Figure S16).[32] Analyses of the headspace for NO gas during the reactions of $NaNO_2$ + $Zn(OTf)_2$ + 2,4-DTBP (or 1,2,4-TMB) also show the formation of NO along with the nitroaromatics (Figures S14 and S15), thereby perhaps indicating an overall disproportionation type transformation involving an N-oxidation state change from +3 (in nitrite) to +5 (in nitro-aromatics) and +2 (in NO). While further mechanistic probing of nitration in the present study remains challenging, these observations suggest that the interaction of nitrite with the Lewis acidic site of the free Zn^{II} salts renders an active electrophilic species, resulting in electrophilic nitration of 2,4-DTBP and 1,2,4-TMB. However, the zinc(II) site in the coordination motif [(**Bn_3Tren**)Zn^{II}]$^{2+}$ is not sufficiently Lewis acidic to activate nitrite toward electrophilic nitration reactions of 2,4-DTBP or 1,2,4-TMB.

Assessment of the Lewis acidity of the metal sites in free Zn^{II} salts versus in the [(**Bn_3Tren**)Zn^{II}]$^{2+}$ coordination motif through the Gutmann−Beckett method provides further insights.[33] Acceptor numbers (AN) of the [Zn^{II}] sites in [(**Bn_3Tren**)Zn^{II}(OTf)](OTf) (**2**) and $Zn^{II}(OTf)_2$ have been

https://doi.org/10.1021/acsorginorgau.3c00004
ACS Org. Inorg. Au 2023, 3, 246−253

determined utilizing triethylphosphine oxide (TEPO) in acetonitrile-d_3 at room temperature (Figures 5, S17, and

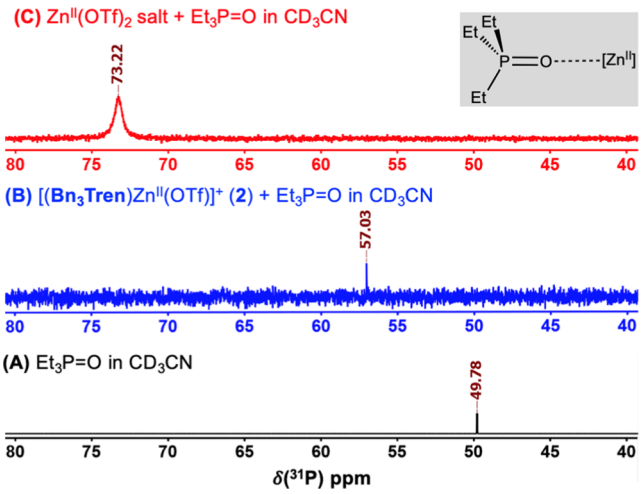

Figure 5. $^{31}P\{^1H\}$ (202 MHz, CD_3CN) NMR spectra of Et_3PO (A), Et_3PO + [(**Bn$_3$Tren**)Zn^{II}(OTf)](OTf) (B), and Et_3PO + Zn^{II}(OTf)$_2$ (C). Inset showing the proposed interaction between the Lewis acidic [Zn^{II}] site and Et_3PO.

Table S2).[34] The downfield chemical shifts of TEPO in $^{31}P\{^1H\}$ and ^1H NMR spectra in the presence of complex **2** or Zn^{II}(OTf)$_2$ relative to free TEPO suggest Lewis acidic interaction between TEPO and the [Zn^{II}] sites. Notably, the experimentally determined acceptor numbers (AN) obtained from the relative $^{31}P\{^1H\}$ chemical shifts were found to be 35.4 (for [(**Bn$_3$Tren**)Zn^{II}]$^{2+}$ in **2**) and 71.2 (for Zn^{II}(OTf)$_2$). This trend of the Lewis acidity not only rationalizes the contrasting reactivity profile of complex **1** versus {$NaNO_2$ + Zn(OTf)$_2$} in the electrophilic aromatic substitution reactions, but also justifies the extent of reactions involving thiol and nitrite in the presence of [(**Bn$_3$Tren**)Zn^{II}]$^{2+}$ site and Zn^{II}(OTf)$_2$ salt (vide supra). Moreover, the above-mentioned studies clearly distinguish that the nucleophilic nature of free nitrite anion in the presence of bare Zn^{II} ions switches to electrophilic, while nitrite anion coordinated at the [(**Bn$_3$Tren**)Zn^{II}]$^{2+}$ site is very mildly electrophilic toward substrates like thiols.

Sulfane Sulfur-Assisted Reactions of Thiol and [Zn^{II}]−Nitrite

As the reaction of alkyl thiol with the modestly electrophilic nitrite moiety in [(**Bn$_3$Tren**)Zn^{II}−nitrite]$^+$ (**1**) is sluggish, leaving a major fraction of nitrite unreacted (Figures 2 and 3), we envisioned to enhance the nucleophilicity of thiol through persulfidation. Reactions of [(**Bn$_3$Tren**)Zn^{II}−nitrite]$^+$ (**1**) with isolated [PPN$^+$][PhSS$^-$]/[PPN$^+$][PhS$_3$S$^-$] in acetonitrile at room temperature afford enhanced yields of NO as 45 and 58%, respectively (Table S1).[35,36] Notably, a reaction of the thiolate anion (from NaSPh) with complex **1** results in NO in 11% yield, which is comparable to that of the thiol reaction (Table S1). Thus, these findings support our hypothesis that the [Zn^{II}]−nitrite moiety in **1** reacts more promptly with the relatively more nucleophilic persulfide anions as compared to the analogous reaction of thiol/thiolate due to the α-effect. Encouraged by our recent report on [Zn^{II}]-promoted thiol persulfidation through thiol and sulfane sulfur cross-talk,[24] we aim to utilize the in situ generated persulfide species for facilitating NO generation from [(**Bn$_3$Tren**)Zn^{II}−nitrite]$^+$ (**1**). Notably, the insertion of the S_3 moiety into the [Zn^{II}]−SAr bond, resulting in the [Zn^{II}]−S_4Ar complex, has been reported previously.[37,38] A comparative reactivity study on the structurally characterized [Zn^{II}]−SAr and [Zn^{II}]−S_4Ar complexes toward alkylation and disulfide addition reactions demonstrates that [Zn^{II}]−S_4Ar is less nucleophilic as compared to [Zn^{II}]−SAr.[39] Thus, this study by Tsui and coworkers illustrated an inverse α-effect in thiolate versus perthiolate reactivity at a [Zn^{II}] site supported by a bis(carboxamide)pyridine ligand.

A reaction of ^{t}BuBnSH (2 equiv) with [(**Bn$_3$Tren**)Zn^{II}−nitrite](ClO$_4$) (**1**) (1 equiv) in the presence of S_8 (8 atom equiv) in acetonitrile at room temperature for 12 h affords a mixture of di-*tert*-butylbenzyl polysulfides (^{t}BuBn−S_n−Bn^{t}Bu, n = 2−5) with a ratio of 0.05:0.46:0.29:0.20 as obtained from the relative integrations of benzyl (Ar−CH_2−) proton resonances of ^{t}BuBn−S_n−Bn^{t}Bu in the NMR spectrum, respectively (Figure S18). ^1H NMR spectroscopic analysis on a crude reaction mixture also reveals complete consumption of thiol. Analysis of headspace on the reaction of (^{t}BuBnSH + complex **1** + S_8) using (TPP)Co^{II} provides NO yield as 65% (Figure S20 and Table S1). Notably, an analogous headspace analysis for the control reaction between complex **1** and S_8 does not produce any NO. A reaction of 4-methylbenzenethiol (4-Me−C_6H_4−SH) with [Zn^{II}]−nitrite complex (**1**) in the presence of S_8 (8 atom equiv) also results in a mixture of diaryl polysulfides as assessed by ^1H NMR (Figure S21). A headspace analysis for NO provides 34% yield of NO, although a Griess assay on the crude reaction mixture suggests complete consumption of nitrite. ^{15}N NMR spectroscopic study on an NMR tube reaction consisting of [(**Bn$_3$Tren**)Zn^{II}−O^{15}NO]$^+$ (**1**-^{15}**N**), S_8, and 4-Me−C_6H_4−SH in CD_3CN depicts a weak but detectable resonance at δ = 540.14 ppm (versus liq. NH_3), consistent with the presence of N-nitrosated ligand (Figure S22).[14] HRMS analysis on the ^{15}N NMR sample confirms the N-nitrosation of the **Bn$_3$Tren** ligand (Figure S22). In contrast, N-nitrosation was not observed for the reactions of less acidic alkyl thiol ^{t}BuBnSH.

Assessing the role of more bio-relevant sulfane sulfur rather than elemental sulfur, a reaction of ^{t}BuBnSH (2 equiv) with [(**Bn$_3$Tren**)Zn^{II}−nitrite](ClO$_4$) (**1**) (1 equiv) in the presence of freshly prepared ^{t}BuBn−S_n−Bn^{t}Bu (n = 2−5) in acetonitrile at room temperature for 12 h leads to an alteration in the initial ratio of polysulfides as indicated by the benzylic proton resonances in the ^1H NMR spectrum (Figure S23). The significant increase in ^{t}BuBnS−SBn^{t}Bu yield indeed hints at the dissimilation of sulfane sulfur from the higher-order sulfides (n > 2). A headspace analysis for NO shows 76% yield (Figure S24, Table S1). Nearly an order of magnitude higher yields of NO from the reactions of thiol and complex **1** in the presence of S_8 or ^{t}BuBn−S_n−Bn^{t}Bu indicates a definitive role of sulfane sulfur in modulating the reactivity of thiol toward [Zn^{II}]−nitrite. The Griess tests on the reaction mixtures (complex **1** + thiol + sulfane sulfurs) suggest more efficient consumptions of nitrite as compared to those for the reactions in the absence of sulfane sulfurs (Table S1). We also turned to probe the coformation of other minor gaseous products such as N_2O and NH_3. Analysis of headspace by FTIR spectroscopy on a gaseous sample shows characteristic vibrational features at 2207 and 2236 cm^{-1} (Figure S25),[40] thereby suggesting the generation of N_2O from [Zn^{II}]−nitrite (**1**) + ^{t}BuBnSH + S_8. Moreover, trapping of headspace in the presence of acid followed by ^1H NMR spectroscopic analysis in DMSO-d_6

https://doi.org/10.1021/acsorginorgau.3c00004
ACS Org. Inorg. Au 2023, 3, 246−253

shows a triplet centered at δ = ~7.18 ppm ($^1J_{NH}$ = 50.3 Hz), which is assigned to NH_4^+ (Figures S26 and S27).[31] The formation of NH_3 from the above reaction may be attributed to the complex reaction between NO and H_2S/HS^-, as suggested in the previous literature.[41]

Evidence of Thiol Persulfidation

As previously demonstrated, 1-fluoro-2,4-dinitrobenzene (F-DNB) has been utilized to probe the presence of a nucleophilic sulfur species like perthiolate (^{t}BuBnSS$^-$) during the course of the reactions.[24,42] Although a reaction between ^{t}BuBnSH and S_8 or ^{t}BuBn−S_n−Bn^{t}Bu in the absence of a [Zn^{II}] site does not afford ^{t}BuBnSS−DNB, the ^{1}H NMR spectrum of the crude mixture consisting of [Zn^{II}]−nitrite (**1**), ^{t}BuBnSH (2 equiv) and sulfane sulfurs in the presence of F-DNB (2 equiv) in acetonitrile at room temperature depicts the formation of ^{t}BuBnSS−DNB in 38% (for S_8) and 46% (for ^{t}BuBn−S_n−Bn^{t}Bu) yields (Table 1 and Figure S28).[24,43] Furthermore,

Table 1. Products (X-DNB, X = ^{t}BuBnS/^{t}BuBnSS) Observed from the Trapping Experiments Using F-DNB

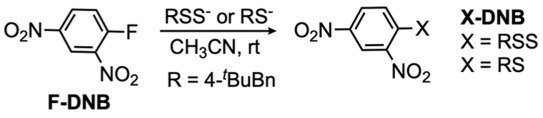

	Reaction	% yield (NMR)	
		RSS-DNB	RS-DNB
1	2RSH + S_8 or R-S_n-R + 2F-DNB	0	0
2	[Zn^{II}]-ONO (**1**) + 2RSH + S_8 + 2F-DNB	38	0
3	[Zn^{II}]-ONO (**1**) + 2RSH + R-S_n-R + 2F-DNB	46	0
4	[Zn^{II}]-ONO (**1**) + 2RSH + 2F-DNB	0	32

high-resolution mass spectrometric (HRMS) analysis on a sample generated from the reaction among [Zn^{II}]−nitrite (**1**) + S_8 + ^{t}BuBnSH in acetonitrile discloses a set of distinct m/z signals with 32 amu gaps appearing at m/z = 691.2829, 723.2551, 755.2272, 787.1990, and 819.1714. These m/z signals with distinct isotopic distribution patterns are congruent with the respective formulations as [(**Bn_3Tren**)-Zn^{II}−S_n−Bn^{t}Bu]$^+$ (calcd m/z = 691.2847, 723.2567, 755.2288, 787.2009, and 819.1729 for n = 2, 3, 4, 5, and 6) (Figures 6, S29 and S30). Hence, these results suggest the in situ generation of the perthiolate species ^{t}BuBnS_n^- during the sulfane sulfur-assisted reaction between the [Zn^{II}]−nitrite complex (**1**) and thiol ^{t}BuBnSH.

Mechanistic Considerations

The reaction of [Zn^{II}]−nitrite (**1**) with thiol and S_8 was monitored by UV−vis spectroscopy to probe the intermediacy of reactive sulfur/nitrogen species such as trisulfur radical anion ($S_3^{\bullet-}$, λ_{max} = 610−620 nm) and perthionitrite ($SSNO^-$, λ_{max} = 440−450 nm).[44−46] It is noteworthy that the NO_2^- anion is known to react with sulfane sulfur species (e.g., S_8, RS_nR, RSSH) to afford ($S_3^{\bullet-}$) and perthionitrite ($SSNO^-$).[47,48] In contrast, UV−vis monitoring of the reactions of [Zn^{II}]−nitrite (**1**) with S_8 or RS_nR does not show any considerable change in the absorption features (Figure S31). Interestingly, addition of thiol ^{t}BuBnSH (2 equiv) to the solution consisting of complex **1** and S_8 (8 at. equiv) in DMF at room temperature results in a growth of a broad absorption feature ranging from

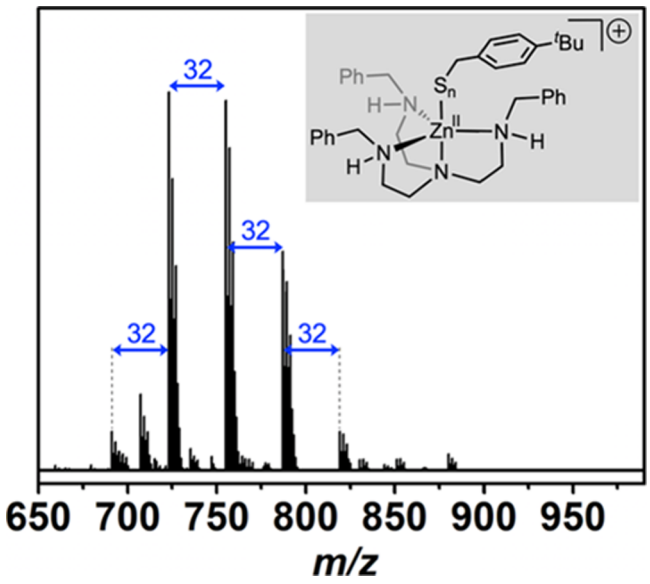

Figure 6. HRMS (ESI+) spectrum showing the m/z peaks for [(**Bn_3Tren**)Zn^{II}−S_n−Bn^{t}Bu]$^+$ (where n = 2, 3, 4, 5, and 6).

300 to 450 nm (Figures S32 and S33). Moreover, unlike in the case for the reaction between [TBA^+][NO_2^-] and S_8, the absence of the distinct features in the ranges of 440−450 and 610−620 nm rules out the generation of $SSNO^-$ and $S_3^{\bullet-}$ as transient intermediates for [Zn^{II}]−nitrite (**1**) + S_8 + ^{t}BuBnSH reactions. Moreover, ^{15}N NMR spectroscopic monitoring of the reaction mixture consisting of [Zn^{II}]−O^{15}NO (**1**-^{15}**N**) + S_8 + ^{t}BuBnSH in CD_3CN does not show any peak assignable to $SS^{15}NO^-$ (Figure S27). The contrast in S_8 reactivity of the NO_2^- anion (in [TBA^+][NO_2^-] salt) versus nitrite coordinated to [Zn^{II}] (in **1**) is attributed to the nucleophilic versus non-nucleophilic reactivity profiles of the nitrite moiety.

Mechanistically, we hypothesize an association between [Zn^{II}]−nitrite (**1**) and sulfane sulfur leading to {[(**Bn_3Tren**)-Zn^{II}−nitrite](S_n)}$^+$ (**Int-a**) (Figure 7, step A). While such an adduct complex could not be identified presently, perhaps due

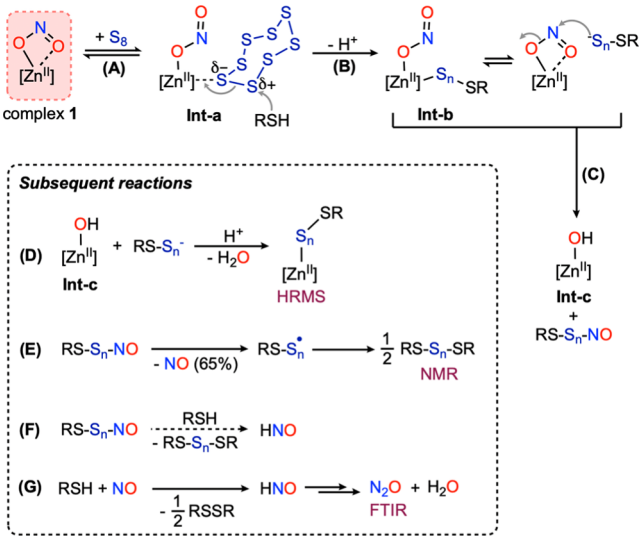

Figure 7. Proposed mechanism for the sulfane sulfur-assisted reactions of thiol and complex **1**. −S_n− indicates a variable number of S-atoms in a linear S−S chain.

https://doi.org/10.1021/acsorginorgau.3c00004
ACS Org. Inorg. Au 2023, 3, 246−253

to the weak association, ESI-MS spectrometric characterization of analogous adducts $\{[(\mathbf{Bn_3Tren})Zn^{II}-Cl](S_n)\}^+$ (n = 4, 5, 6, 7, 8) has been recently demonstrated for the reaction of the $[(\mathbf{Bn_3Tren})Zn^{II}-Cl]^+$ complex with S_8.[24] Such an interaction between sulfane sulfur and the $[Zn^{II}]$ site (in **Int-a**) is proposed to result in a weak polarization of the S−S bond, thereby facilitating the intermolecular nucleophilic attack by thiol RSH, leading to a perthiolate species RS_nS^- (Figure 7, step B). Subsequently, RS_nS^- species is proposed to attack as a strong nucleophile on the mildly electrophilic nitrite moiety at the $[Zn^{II}]$ site in complex **1** to yield $[Zn^{II}]$-hydroxide (**Int-c**) species and transient RS_nSNO (Figure 7, step C).[49] This proposed step is consistent with the analogous reaction between $[Zn^{II}]$−nitrite and thiol leading to $[Zn^{II}]$-hydroxide species and RSNO (Figure 2). At the same time, $[Zn^{II}]$-bound perthiolate in **Int-b** may also exhibit nucleophilic reactivity, leading to an intramolecular attack on the $[Zn^{II}]$−ONO moiety to afford $[Zn^{II}]$-hydroxide and RS_nSNO.[50] The proposed $[Zn^{II}]$-hydroxide species (**Int-c**) undergoes reaction with RSH/RS_nSH to yield $[Zn^{II}]-S_nR$ as identified through HRMS analyses (Figure 7, step D; Figures S29, S30 and S34−S36). Anticipating an extremely weak S−N bond in RS_nS-NO, homolysis of the S−N bond is likely to yield NO and $RS_nS^\bullet$ (Figure 7, step E).[48,49] Subsequently, $RS_nS^\bullet$ is proposed to undergo radical coupling to provide organic polysulfide RSS_nSR (Figure 7, step E). An alternative pathway considering the S−N bond heterolysis of RS_nS-NO in the presence of nucleophiles (e.g., RSH/RS_nSH or their conjugate base) could provide transient nitroxyl (HNO) prior to a rapid dimerization to release N_2O (Figure 7, step F).[51] As described in the literature,[48,49] however, RS_nS-NO species is more likely to undergo S−N bond homolysis spontaneously rather than heterolysis. Moreover, the findings of NO as the major product from nitrite also suggest that the S−N bond homolysis of RS_nS-NO is the major route under the present reaction conditions. The minor amount of N_2O may be attributed via HNO, which is known to generate from RSH and NO (Figure 7, step G).[52] Although H_2S/HS^- (37% yield) has been reported previously for $\{[\mathbf{Bn_3Tren}]Zn^{II}\text{-aqua}\}(ClO_4)_2$ mediated reaction of thiol and S_8,[24] only a trace amount of H_2S/HS^- has been identified for the reactions of $[Zn^{II}]$−nitrite (**1**) + S_8 + ^{t}BuBnSH (2 equiv) as evaluated by the methylene blue (MB) assay.[53] The poor yield of H_2S/HS^- is attributed to a reaction between NO and H_2S/HS^- leading to the formation of a minor amount of NH_3 (vide supra).

CONCLUSIONS

To conclude, this report illustrates that the efficiency of NO generation from the interaction of thiol and nitrite at a $[Zn^{II}]$ site depends on the Lewis acidity of the $[Zn^{II}]$ site as established by the Gutmann−Beckett method. Owing to the redox-inactive nature of the $[Zn^{II}]$ site, the initial interaction between $[Zn^{II}]$−nitrite and the thiol providing RSNO is redox-neutral. Subsequently, thermal decomposition of RSNO to RSSR and NO is responsible for the overall 1e$^-$ redox process associated with the nitrite-to-NO transformation. Consistent with the previous report,[13] the reactions of nitrite-bound tripodal model complexes of CA with 1° alkyl thiols were found to be slow and suffer from poor conversion. Interestingly, the present study outlines that sulfane sulfur species such as S_8 and RS_nR (n > 2) facilitate the reactions of 1° alkyl thiol and $[Zn^{II}]$-bound nitrite species through the intermediacy of more nucleophilic perthiolate species RS_nS^-. 1-Fluoro-2,4-dinitrobenzene (F-DNB) has been successfully utilized to probe the in situ generated metastable perthiolate as RSS−DNB. A set of complementary analyses involving UV−vis, FTIR, NMR, and HRMS support the mechanistic hypothesis, which is distinct as compared to the previously illustrated route for free nitrite salt $[TBA^+][NO_2^-]$ and sulfane sulfurs.[48] The variations in the underlying reaction pathways have been discussed in line with the reactivity trends of the nitrite moiety as uncoordinated versus metal-bound forms. The insights gained from this study may urge considering the involvements of various biologically relevant sulfane sulfur (S^0) species in nitrite-to-NO conversion at $[Zn^{II}]$-containing active sites such as in carbonic anhydrase (CA), zinc fingers, and cysteinyl-tRNA synthetase.[53−56]

EXPERIMENTAL SECTION

General Procedure for the Reactions of Nitrite and Thiols at Zinc(II) Sites

In a N_2-filled glovebox, thiol (^{t}BuBnSH or 4-Me−C_6H_4−SH) (0.080 mmol, 1.0 equiv) was added to a solution of $[(\mathbf{Bn_3Tren})Zn^{II}-\text{nitrite}](ClO_4)$ (**1**) or a 1:1 mixture of $NaNO_2$ and $Zn(OTf)_2$ (0.080 mmol, 1.0 equiv) in acetonitrile (~4 mL). The color of the reaction mixture turned pink or brownish green upon stirring at room temperature due to the formation of the corresponding *S*-nitrosothiol (RSNO, R = ^{t}BuBn and 4-Me−C_6H_4), respectively. After 8 h, the solvent was removed under reduced pressure. For ^{t}BuBnSH reactions, the resultant crude reaction mixture was analyzed by ^{1}H NMR. Relative integration of the benzyl−CH_2− protons provided the estimation of thiol consumption and yields of *S*-nitrosothiol and disulfide. For Me−C_6H_4−SH reactions, the crude solid obtained after the removal of the solvent was treated with hexane (4 × 5 mL) for extracting organic products from the crude. An aliquot of the combined hexane extracts was directly analyzed by GCMS for the estimation of unreacted thiol. The hexane extracts were also dried and analyzed by ^{1}H NMR for the characterization of the thiol-derived products. *S*-nitrosothiol products were characterized by comparing their spectroscopic (UV−vis, NMR, and FTIR) signatures.

General Procedure for the Reactions of Nitrite and Thiols at Zinc(II) Sites in the Presence of Sulfane Sulfurs

Elemental sulfur S_8 (0.655 mmol of S, 8 at. equiv) or a freshly prepared[24] mixture of organic polysulfides ^{t}BuBn−S_n−Bn^{t}Bu (n = 2, 3, 4, >4) (0.080 mmol) and thiol ^{t}BuBnSH (0.160 mmol, 2.0 equiv) were added consecutively to a solution of $[(\mathbf{Bn_3Tren})Zn^{II}-\text{nitrite}](ClO_4)$ (**1**) in acetonitrile (~5 mL) under a N_2 atmosphere of a glovebox. The reaction mixture was allowed to stir at room temperature for 12 h. The resultant solution was then filtered, and the filtrate was dried under reduced pressure. The crude solid was treated with hexane (4 × 5 mL) and filtered to combine the hexane layers for extracting the organic polysulfide mixture from the crude. The combined hexane extracts were evaporated to dryness to obtain a pale yellow semi-solid, which was analyzed by ^{1}H NMR. The relative integrations of the benzyl protons Ar−CH_2− provided the relative ratio of different polysulfides ^{t}BuBn−S_n−Bn^{t}Bu (n = 2−5).

The reaction of complex **1** and 4-Me−C_6H_4−SH in the presence of S_8 was performed and analyzed similarly as described above.

Estimation of NO and Unreacted Nitrite (NO_2^-)

The headspaces on the reactions of nitrite and thiol were carried out for the quantification of NO gas after trapping the evolved gas as (TPP)Co(NO)[23] utilizing a "H-setup" (Scheme S2 and Section S9 in the Supporting Information). Griess analyses,[28] for quantifying the unreacted nitrite after the reactions, were performed on the (nitrite + thiol) reaction mixtures as obtained from the NO-trapping experiments (Section S10 in Supporting Information).

https://doi.org/10.1021/acsorginorgau.3c00004
ACS Org. Inorg. Au 2023, 3, 246−253

■ ASSOCIATED CONTENT

Data Availability Statement

The data underlying this study are available in the published article and its Supporting Information.

Supporting Information

The Supporting Information is available free of charge at https://pubs.acs.org/doi/10.1021/acsorginorgau.3c00004.

General instrumentation methods and experimental details including characterization data (PDF)

■ AUTHOR INFORMATION

Corresponding Author

Subrata Kundu − *School of Chemistry, Indian Institute of Science Education and Research Thiruvananthapuram (IISER-TVM), Thiruvananthapuram 695551, India;* orcid.org/0000-0002-3533-3206; Email: skundu@iisertvm.ac.in, skundu.chem@gmail.com

Authors

Tuhin Sahana − *School of Chemistry, Indian Institute of Science Education and Research Thiruvananthapuram (IISER-TVM), Thiruvananthapuram 695551, India*

Adwaith K. Valappil − *School of Chemistry, Indian Institute of Science Education and Research Thiruvananthapuram (IISER-TVM), Thiruvananthapuram 695551, India*

Anaswar S. P. R. Amma − *School of Chemistry, Indian Institute of Science Education and Research Thiruvananthapuram (IISER-TVM), Thiruvananthapuram 695551, India*

Complete contact information is available at: https://pubs.acs.org/10.1021/acsorginorgau.3c00004

Author Contributions

CRediT: **Tuhin Sahana** data curation (lead), formal analysis (lead), investigation (lead), writing-review & editing (supporting); **Adwaith K. Valappil** formal analysis (supporting), investigation (supporting), writing-review & editing (supporting); **Anaswar S. P. R. Amma** formal analysis (supporting), investigation (supporting); **Subrata Kundu** conceptualization (lead), data curation (supporting), formal analysis (supporting), funding acquisition (lead), project administration (lead), resources (lead), supervision (lead), writing-original draft (equal).

Notes

The authors declare no competing financial interest.

■ ACKNOWLEDGMENTS

S.K. gratefully acknowledges the Core Research grant (CRG/2021/001174) from SERB. The authors are also thankful to IISER Thiruvananthapuram for support.

■ REFERENCES

(1) Gladwin, M. T.; Schechter, A. N.; Kim-Shapiro, D. B.; Patel, R. P.; Hogg, N.; Shiva, S.; Cannon, R. O.; Kelm, M.; Wink, D. A.; Espey, M. G.; Oldfield, E. H.; Pluta, R. M.; Freeman, B. A.; Lancaster, J. R.; Feelisch, M.; Lundberg, J. O. The Emerging Biology of the Nitrite Anion. *Nat. Chem. Biol.* **2005**, *1*, 308−314.

(2) Maia, L. B.; Moura, J. J. G. How Biology Handles Nitrite. *Chem. Rev.* **2014**, *114*, 5273−5357.

(3) Palacios-callender, M.; Hollis, V.; Mitchison, M.; Frakich, N.; Unitt, D.; Moncada, S. Cytochrome c Oxidase Regulates Endogenous Nitric Oxide Availability in Respiring Cells: A Possible Explanation for Hypoxic Vasodilation. *Proc. Natl. Acad. Sci. U.S.A.* **2007**, *104*, 18508−18513.

(4) Merkle, A. C.; Lehnert, N. Binding and Activation of Nitrite and Nitric Oxide by Copper Nitrite Reductase and Corresponding Model Complexes. *Dalton Trans.* **2012**, *41*, 3355−3368.

(5) Cosby, K.; Partovi, K. S.; Crawford, J. H.; Patel, R. P.; Reiter, C. D.; Martyr, S.; Yang, B. K.; Waclawiw, M. A.; Zalos, G.; Xu, X.; Huang, K. T.; Shields, H.; Kim-shapiro, D. B.; Schechter, A. N.; Cannon, R. O. C.; Gladwin, M. T. Nitrite Reduction to Nitric Oxide by Deoxyhemoglobin Vasodilates the Human Circulation. *Nat. Med.* **2003**, *9*, 1498−1505.

(6) Li, H.; Samouilov, A.; Liu, X.; Zweier, J. L. Characterization of the Magnitude and Kinetics of Xanthine Oxidase-Catalyzed Nitrite Reduction. *J. Biol. Chem.* **2001**, *276*, 24482−24489.

(7) Aamand, R.; Dalsgaard, T.; Jensen, F. B.; Simonsen, U.; Roepstorff, A.; Fago, A. Generation of Nitric Oxide from Nitrite by Carbonic Anhydrase: A Possible Link between Metabolic Activity and Vasodilation. *Am. J. Physiol.* **2009**, *297*, 2068−2074.

(8) Nielsen, P. M.; Fago, A. Inhibitory Effects of Nitrite on the Reactions of Bovine Carbonic Anhydrase II with CO2 and Bicarbonate Consistent with Zinc-Bound Nitrite. *J. Inorg. Biochem.* **2015**, *149*, 6−11.

(9) Pickerodt, P. A.; Kronfeldt, S.; Russ, M.; Gonzalez-Lopez, A.; Lother, P.; Steiner, E.; Vorbrodt, K.; Busch, T.; Boemke, W.; Francis, R. C. E.; Swenson, E. R. Carbonic Anhydrase Is Not a Relevant Nitrite Reductase or Nitrous Anhydrase in the Lung. *J. Physiol.* **2019**, *597*, 1045−1058.

(10) Wang, L.; Sparacino-Watkins, C. E.; Wang, J.; Wajih, N.; Varano, P.; Xu, Q.; Cecco, E.; Tejero, J.; Soleimani, M.; Kim-Shapiro, D. B.; Gladwin, M. T. Carbonic Anhydrase II Does Not Regulate Nitrite-Dependent Nitric Oxide Formation and Vasodilation. *Br. J. Pharmacol.* **2020**, *177*, 898−911.

(11) Andring, J. T.; Lomelino, C. L.; Tu, C.; Silverman, D. N.; McKenna, R.; Swenson, E. R. Carbonic Anhydrase II Does Not Exhibit Nitrite Reductase or Nitrous Anhydrase Activity. *Free Radical Biol. Med.* **2018**, *117*, 1−5.

(12) Hanff, E.; Böhmer, A.; Zinke, M.; Gambaryan, S.; Schwarz, A.; Supuran, C. T.; Tsikas, D. Carbonic Anhydrases Are Producers of S-Nitrosothiols from Inorganic Nitrite and Modulators of Soluble Guanylyl Cyclase in Human Platelets. *Amino Acids* **2016**, *48*, 1695−1706.

(13) Cardenas, A. J. P.; Abelman, R.; Warren, T. H. Conversion of Nitrite to Nitric Oxide at Zinc via *S*-Nitrosothiols. *Chem. Commun.* **2014**, *50*, 168−170.

(14) Kundu, S.; Kim, W. Y.; Bertke, J. A.; Warren, T. H. Copper(II) Activation of Nitrite: Nitrosation of Nucleophiles and Generation of NO by Thiols. *J. Am. Chem. Soc.* **2017**, *139*, 1045−1048.

(15) Khin, C.; Heinecke, J.; Ford, P. C. Oxygen Atom Transfer from Nitrite Mediated by Fe(III) Porphyrins in Aqueous Solution. *J. Am. Chem. Soc.* **2008**, *130*, 13830−13831.

(16) Sanders, B. C.; Hassan, S. M.; Harrop, T. C. NO_2^- Activation and Reduction to NO by a Nonheme $Fe(NO_2)_2$ Complex. *J. Am. Chem. Soc.* **2014**, *136*, 10230−10233.

(17) Timmons, A. J.; Symes, M. D. Converting between the Oxides of Nitrogen Using Metal-Ligand Coordination Complexes. *Chem. Soc. Rev.* **2015**, *44*, 6708−6722.

(18) Sakhaei, Z.; Kundu, S.; Donnelly, J. M.; Bertke, J. A.; Kim, W. Y.; Warren, T. H. Nitric Oxide Release via Oxygen Atom Transfer from Nitrite at Copper(II). *Chem. Commun.* **2017**, *53*, 549−552.

(19) Gwak, J.; Ahn, S.; Baik, M. H.; Lee, Y. One Metal Is Enough: A Nickel Complex Reduces Nitrate Anions to Nitrogen Gas. *Chem. Sci.* **2019**, *10*, 4767−4774.

(20) Kulbir; Das, S.; Devi, T.; Goswami, M.; Yenuganti, M.; Bhardwaj, P.; Ghosh, S.; Chandra Sahoo, S.; Kumar, P. Oxygen Atom Transfer Promoted Nitrate to Nitric Oxide Transformation: A Step-

Wise Reduction of Nitrate → Nitrite → Nitric Oxide. *Chem. Sci.* **2021**, *12*, 10605−10612.
(21) Mondal, A.; Reddy, K. P.; Bertke, J. A.; Kundu, S. Phenol Reduces Nitrite to NO at Copper(II): Role of a Proton-Responsive Outer Coordination Sphere in Phenol Oxidation. *J. Am. Chem. Soc.* **2020**, *142*, 1726−1730.
(22) Chang, Y.-L.; Chen, H.-Y.; Chen, S.-H.; Kao, C.-L.; Chiang, M. Y.; Hsu, S. C. N. An Investigation on Catalytic Nitrite Reduction Reaction by Bioinspired Cu^{II} Complexes. *Dalton Trans.* **2022**, *51*, 7715−7722.
(23) Gupta, S.; Vijayan, S.; Bertke, J. A.; Kundu, S. NO Generation from the Cross-Talks between Ene-Diol Antioxidants and Nitrite at Metal Sites. *Inorg. Chem.* **2022**, *61*, 8477−8483.
(24) Sahana, T.; Kakkarakkal, D. C.; Kundu, S. Cross-Talks Between Sulfane Sulfur and Thiol at a Zinc(II) Site. *Chem.—Eur. J.* **2022**, *28*, No. e202200776.
(25) Williams, D. L. H. The Chemistry of S-Nitrosothiols. *Acc. Chem. Res.* **1999**, *32*, 869−876.
(26) Hosseininasab, V.; Mcquilken, A. C.; Bakhoda, A. G.; Bertke, J. A.; Timerghazin, Q. K.; Warren, T. H. Lewis Acid Coordination Redirects S-Nitrosothiol Signaling Output. *Angew. Chem., Int. Ed.* **2020**, *59*, 10854−10858.
(27) Chivers, T.; Laitinen, R. S. *Chalcogen-Nitrogen Chemistry: From Fundamentals to Applications in Biological, Physical and Materials Sciences*; World Scientific, 2021.
(28) Griess tests for the estimation of unreacted nitrite present in the reaction mixtures were carried out by following a modified protocol as described elsewhere Hong, S.; Kumar, P.; Cho, K.; Lee, Y.; Karlin, K. D.; Nam, W. Mechanistic Insight into the Nitric Oxide Dioxygenation Reaction of Nonheme Iron(III)−Superoxo and Manganese(IV)−Peroxo Complexes. *Angew. Chem., Int. Ed.* **2016**, *55*, 12403−12407.
(29) Coelho, S. E.; Schneider, F. S. S.; de Oliveira, D. C.; Tripodi, G. L.; Eberlin, M. N.; Caramori, G. F.; de Souza, B.; Domingos, J. B. Mechanism of Palladium(II)-Mediated Uncaging Reactions of Propargylic Substrates. *ACS Catal.* **2019**, *9*, 3792−3799.
(30) ^{15}N NMR chemical shift (versus liquid NH_3) of $RO^{15}NO$ ranges around 585 ppm. See ref 14.
(31) Sahana, T.; Mondal, A.; Anju, B. S.; Kundu, S. Metal-free Transformations of Nitrogen-Oxyanions to Ammonia via Oxoammonium Salt. *Angew. Chem., Int. Ed.* **2021**, *60*, 20661−20665.
(32) Craik, D. J.; Levy, G. C.; Brownlee, R. T. C. Substituent Effects on ^{15}N and ^{17}O Chemical Shifts in Nitrobenzenes: Correlations with Electron Densities. *J. Org. Chem.* **1983**, *48*, 1601−1606.
(33) Gutmann, V. Solvent Effects on the Reactivities of Organometallic Compounds. *Coord. Chem. Rev.* **1976**, *18*, 225−255.
(34) Geri, J. B.; Shanahan, J. P.; Szymczak, N. K. Testing the Push−Pull Hypothesis: Lewis Acid Augmented N_2 Activation at Iron. *J. Am. Chem. Soc.* **2017**, *139*, 5952−5956.
(35) Thiolate and perthiolate salts of the parent thiol PhSH instead of ^{t}BuBnSH have been used due to the relatively more stable nature of PhS_nS^- as compared to the benzyl analogues.
(36) $[PPN^+][PhSS^-]$ and $[PPN^+][PhS_3S^-]$ salts were isolated following the previously reported literature Jungen, S.; Paenurk, E.; Chen, P. Synthesis, Spectroscopic, and Structural Characterization of Organyl Disulfanides and a Tetrasulfanide. *Inorg. Chem.* **2020**, *59*, 12322−12336.
(37) Ballesteros, M., II.; Tsui, E. Y. Sulfur Transfer Reactions of a Zinc Tetrasulfanido Complex. *Dalton Trans.* **2020**, *49*, 16305−16311.
(38) Ballesteros, M., II.; Tsui, E. Y. Reactivity of Zinc Thiolate Bonds: Oxidative Organopolysulfide Formation and S3 Insertion. *Inorg. Chem.* **2019**, *58*, 10501−10507.
(39) Seo, W. M.; Ballesteros, M. I.; Tsui, E. Y. Sulfane Decreases the Nucleophilic Reactivity of Zinc Thiolates: Implications for Biological Reactive Sulfur Species. *J. Am. Chem. Soc.* **2022**, *144*, 20630−20640.
(40) Mondal, A.; Reddy, K. P.; Som, S.; Chopra, D.; Kundu, S. Nitrate and Nitrite Reductions at Copper(II) Sites: Role of Noncovalent Interactions from Second-Coordination-Sphere. *Inorg. Chem.* **2022**, *61*, 20337−20345.
(41) Ivanovic-Burmazovic, I.; Filipovic, M. R. Saying NO to H_2S: A Story of HNO, HSNO, and SSNO-. *Inorg. Chem.* **2019**, *58*, 4039−4051.
(42) Bora, P.; Chauhan, P.; Manna, S.; Chakrapani, H. A Vinyl-Boronate Ester-Based Persulfide Donor Controllable by Hydrogen Peroxide, a Reactive Oxygen Species (ROS). *Org. Lett.* **2018**, *20*, 7916−7920.
(43) F-DNB experiment for the reaction of $[Zn^{II}]$−nitrite (**1**), ^{t}BuBnSH (2 equiv), sulfane sulfur, and F-DNB (2 equiv) does not show the formation of 2,4-dinitrophenol (Figure S13), thereby ruling out the presence of uncoordinated nitrite anion during the course of the reaction.
(44) Steudel, R.; Chivers, T. The Role of Polysulfide Dianions and Radical Anions in the Chemical, Physical and Biological Sciences, Including Sulfur-Based Batteries. *Chem. Soc. Rev.* **2019**, *48*, 3279−3319.
(45) Chivers, T.; Elder, P. J. W. Ubiquitous Trisulfur Radical Anion: Fundamentals and Applications in Materials Science, Electrochemistry, Analytical Chemistry and Geochemistry. *Chem. Soc. Rev.* **2013**, *42*, 5996−6005.
(46) Marcolongo, J. P.; Venâncio, M. F.; Rocha, W. R.; Doctorovich, F.; Olabe, J. A. NO/H2S "Crosstalk" Reactions. The Role of Thionitrites (SNO-) and Perthionitrites (SSNO-). *Inorg. Chem.* **2019**, *58*, 14981−14997.
(47) Seel, F.; Kuhn, R. G.; Simon, G.; Wagner, M.; Krebs, B.; Dartmann, M. Z. PNP-Perthionitrit und PNP-Monothionitrit/PNP-Perthionitrite and PNP-Monothionitrite. *Naturforsch., B: J. Chem. Sci.* **1985**, *40*, 1607−1617.
(48) Bailey, T. S.; Henthorn, H. A.; Pluth, M. D. The Intersection of NO and H_2S: Persulfides Generate NO from Nitrite through Polysulfide Formation. *Inorg. Chem.* **2016**, *55*, 12618−12625.
(49) Zarenkiewicz, J.; Perez-ternero, C.; Kojasoy, V.; Mcginity, C.; Khodade, V. S.; Lin, J.; Tantillo, D. J.; Toscano, J. P.; Hobbs, A. J.; Fukuto, J. M. The Reaction of Hydropersulfides (RSSH) with S-Nitrosothiols (RS-NO) and the Biological/Physiological Implications. *Free Radical Biol. Med.* **2022**, *188*, 459−467.
(50) Boerzel, H.; Koeckert, M.; Bu, W.; Spingler, B.; Lippard, S. J. Zinc-Bound Thiolate-Disulfide Exchange: A Strategy for Inhibiting Metallo-β-Lactamases. *Inorg. Chem.* **2003**, *42*, 1604−1615.
(51) Doctorovich, F.; Bikiel, D. E.; Suárez, S. A.; Marcelo, A. How to Find an HNO Needle in a (Bio)-Chemical Haystack. *Prog. Inorg. Chem.* **2014**, *58*, 145−184.
(52) Suarez, S. A.; Muñoz, M.; Alvarez, L.; Venâncio, M. F.; Rocha, W. R.; Bikiel, D. E.; Marti, M. A.; Doctorovich, F. HNO Is Produced by the Reaction of NO with Thiols. *J. Am. Chem. Soc.* **2017**, *139*, 14483−14487.
(53) Saju, A.; Mondal, A.; Chattopadhyay, T.; Kolliyedath, G.; Kundu, S. H_2S Generation from CS_2 Hydrolysis at a Dinuclear Zinc(II) Site. *Inorg. Chem.* **2020**, *59*, 16154−16159.
(54) Parkin, G. Synthetic Analogues Relevant to the Structure and Function of Zinc Enzymes. *Chem. Rev.* **2004**, *35*, 699−767.
(55) Laity, J. H.; Lee, B. M.; Wright, P. E. Zinc Finger Proteins: New Insights into Structural and Functional Diversity. *Curr. Opin. Struct. Biol.* **2001**, *11*, 39−46.
(56) Kasamatsu, S. Persulfides-Dependent Regulation of Electrophilic Redox Signaling in Neural Cells. *Antioxid. Redox Signaling* **2020**, *33*, 1320−1331.

https://doi.org/10.1021/acsorginorgau.3c00004
ACS Org. Inorg. Au 2023, 3, 246−253